Electronic Properties and Solid-State ^{87}Rb and ^{13}C NMR Studies of Mesoporous Tantalum Oxide Rubidium Fulleride Composites

Boris O. Skadtchenko,† Michel Trudeau,‡ Robert W. Schurko,*,† Andy Y. H. Lo,† and David M. Antonelli*,†

Department of Chemistry and Biochemistry, University of Windsor, 401 Sunset Avenue, Windsor, Ontario N9B 3P4, and M. L. Trudeau, Emerging Technologies, Hydro-Québec Research Institute, 1800 Boul. Lionel-Boulet, Varennes, Quebec J3X 1S1, Canada

Received October 18, 2004. Revised Manuscript Received November 25, 2004

Mesoporous tantalum oxide rubidium fulleride composites were synthesized by solution impregnation and characterized by elemental analysis, X-ray diffraction, Raman spectroscopy, nitrogen adsorption/desorption, X-ray photoelectron spectroscopy, superconducting quantum interference device magnetometry, room- and variable-temperature electron transport measurements, and solid-state ^{87}Rb and ^{13}C NMR. The room-temperature conductivity pattern, as a function of the oxidation state of C_{60}^{n-}, displayed a conductivity minimum at $n = 3.0$ and a single maximum at $n = 4.0$, while variable-temperature conductivity measurements indicated that the $n = 1.0$ composite is a semiconductor and the $n = 4.0$ material is a narrow band gap semiconductor or a semimetal. Solid-state ^{87}Rb NMR of the composite materials indicated the presence of two Rb environments associated with the walls or channels of the mesostructure as well as several resonances associated with various fulleride species. The $n = 3.0$ and $n = 4.0$ samples showed a substantial increase of Rb ions confined into the walls of mesostructure as well as the buildup of a Rb environment associated with a fulleride species. Solid-state ^{13}C NMR experiments showed the presence of multiple fulleride species as well as pure fullerene, depending on the level of reduction.

Introduction

Mesoporous materials[1−9] have recently attracted much attention due to their ability to act as scaffolding for the construction of low-dimensional nanophases which would otherwise be unstable and prone to structural collapse or grain growth without the structural support imparted by the walls of the mesostructure.[10−12] In this regard the mesoporous framework can act as a "nanoscale test tube" to isolate and study low-dimensional systems in an environment where spectroscopic and structural studies are more facile due to the increased stability of the nanophase of interest. To this end we have used mesoporous titanium, niobium, and tantalum oxides as a support for one-dimensional alkali-metal fulleride nanowires.[13−17] In the bulk phase, alkali-metal fullerides of the general formula A_3C_{60} (A = Na, K, Rb, Cs) adopt an fcc structure and display superconducting properties for many phases at temperatures of 33 K or lower.[18−21] The room-temperature metallic behavior and source of superconductivity are not fully understood because the materials should be Mott−Hubbard insulators, as they possess a half-filled t_{1u} band.[22] As a result, it is widely believed that these materials contain oxidation state defects and are best viewed as hole-doped Mott−Hubbard insulators, although this has been difficult to prove unequivocally by

† University of Windsor.
‡ Hydro-Québec Research Institute.

(1) Beck, J. S.; Vartuli, J. C.; Roth, W. J.; Leonowicz, M. E.; Kresge, C. T.; Schmitt, K. D.; Chu, C. T.-W.; Olson, D. H.; Shepard, E. W.; McCullen, S. B.; Higgins, J. B.; Schlenker, J. L. J. *J. Am. Chem. Soc.* **1992**, *114*, 10834.
(2) Kresge, C. T.; Leonowicz, M. E.; Roth, W. J.; Vartulli, J. C.; Beck, J. S. *Nature* **1992**, *359*, 710.
(3) Antonelli, D. M.; Ying, J. Y. *Angew. Chem., Int. Ed. Engl.* **1995**, *34*, 2014.
(4) Antonelli, D. M.; Ying, J. Y. *Angew. Chem., Int. Ed. Engl.* **1996**, *35*, 426.
(5) Antonelli, D. M.; Ying, J. Y. *Chem. Mater.* **1996**, *8*, 874.
(6) Huo, Q.; Margolese, D. I.; Ciesla, U.; Demuth, D. G.; Feng, P.; Gier, T. E.; Sieger, P.; Firouzi, A.; Chmelka, B. F.; Schuth, F.; Stucky, G. D. *Chem. Mater.* **1994**, *6*, 1176.
(7) Huo, Q.; Margolese, D. I.; Ciesla, U.; Feng, P.; Gier, T. E.; Sieger, P.; Leon, R.; Petroff, P. M.; Schuth, F.; Stucky, G. D. *Nature* **1994**, *368*, 317.
(8) Tanev, P. N.; Chibwe, M.; Pinnavaia, T. J. *Nature* **1994**, *368*, 321.
(9) Antonietti, M.; Berton, B.; Goeltner, C.; Hentze, H. *Adv. Mater.* **1998**, *10*, 154.
(10) Roth, S.; Mahler, G.; Shen, Y.; Cotter, F. *Synth. Met.* **1989**, *28*, 815.
(11) Carter, C. *Molecular Electronic Devices*; Marcel Dekker: New York, 1982.
(12) Antonelli, D. M. *Adv. Mater.* **1999**, *11*, 487.
(13) Ye, B.; Trudeau, M.; Antonelli, D. M. *Adv. Mater.* **2001**, *12*, 29.
(14) Ye, B.; Trudeau, M.; Antonelli, D. M. *Adv. Mater.* **2001**, *13*, 561.
(15) Ye, B.; Trudeau, M.; Antonelli, D. M. *Chem. Mater.* **2001**, *13*, 2730.
(16) Ye, B.; Trudeau, M.; Antonelli, D. M. *Chem. Mater.* **2002**, *14*, 2774.
(17) Skadtchenko, B. O.; Trudeau, M.; Schurko, R. W.; Willans, M. J.; Antonelli, D. M. *Adv. Funct. Mater.* **2003**, *13*, 671.
(18) Haddon, R. C.; Hebard, A. F.; Rosseinsky, M. J.; Murphy, D. W.; Duclos, S. J.; Lyons, K. B.; Miller, B.; Rosamilia, J. M.; Fleming, R. M.; Kortan, A. R.; Glarum, S. H.; Makhija, A. V.; Muller, A. J.; Eick, R. H.; Zahurak, S. M.; Tycko, R.; Dabbagh, G.; Thiel, F. A. *Nature* **1991**, *350*, 320.
(19) Hebard, A. F.; Rosseinsky, M. J.; Haddon, R. C.; Murphy, D. W.; Glarum, S. H.; Palstra, T. T. M.; Ramirez, A. P.; Kortan, A. R. *Nature* **1991**, *350*, 600.
(20) Holczer, K.; Klein, O.; Huang, S. M.; Kaner, R. B.; Fu, K. J.; Whetten, R. L.; Dederich, F. *Science* **1991**, *252*, 1154.
(21) Tanigaki, K.; Ebbesen, T. W.; Saito, S.; Mizuki, J.; Tsai, J.; Kubo, Y.; Kuroshima, S. *Nature* **1991**, *352*, 222.
(22) Mott, N. F. *Metal-Insulator Transition*, 2nd ed.; Taylor & Francis: London, 1999.

10.1021/cm048174t CCC: $30.25
Published on Web 02/17/2005

any means of characterization.[23] Recent advances, however, indicated that the triple degeneracy of the t_{1u} band may lead to the removal of strong electron repulsion, the key factor of the Mott−Hubbard model, and thus might be responsible for metallic and superconducting behavior in A_3C_{60}-type fullerides.[24] To gain further information on the role of the oxidation state in conductivity as well as the effect of diminishing dimensions on alkali-metal fullerides in general, we studied the electronic properties of one-dimensional sodium, potassium, and lithium fulleride nanowires in mesoporous titanium, niobium, and tantalum oxide hosts as a function of reduction, while using the ^{23}Na and ^{7}Li nuclei as NMR probes to elucidate the local structure within the pores.[17,25] Contrary to what is observed for bulk fullerides, mesoporous composites of K_nC_{60} ($n = 0.5-2.5$) and Na_nC_{60} ($n = 0.5$) are semiconductors, those with $n = 3.0$ (K, Na) are insulators, and those with $n \approx 4$ (K, Na) are metals or semimetals.[15,17] The term "*n*" refers to the mean oxidation state of the fulleride in the composite as measured by the position of the Raman A_g band.

All lithium fulleride composites synthesized are insulating, while the sodium fulleride composites studied previously by our group are semiconductors. The source of metallic behavior in the potassium fulleride composites is of much interest but is not yet understood, as the $n = 4.0$ phase in bulk fullerides is insulating. Because rubidium fullerides possess a higher T_c than potassium fullerides (lithium and sodium fullerides are not superconducting) and ^{87}Rb is an extremely useful NMR probe (much larger shift range than ^{23}Na NMR and much higher receptivity than ^{39}K NMR), we chose to synthesize and investigate a new series of mesoporous tantalum oxide rubidium fulleride composites in hope that we could gain more insight into the relationship between local structure and the unusual conductivity patterns in this class of materials.

Experimental Section

Materials and Equipment. All chemicals unless otherwise stated were obtained from Aldrich. Samples of mesoporous tantalum oxide were used without further purification.[5] Trimethylsilyl chloride was distilled over calcium hydride. Mesoporous tantalum oxide was dried at 100 °C overnight under vacuum and then stirred with excess trimethylsilyl chloride in dry ether for 12 h under nitrogen. Nitrogen adsorption and desorption data were collected on a Micromeritics ASAP 2010. X-ray diffraction (XRD) patterns (Cu Kα) were recorded in a sealed glass capillary on a Bruker AXS D8-Discover diffractometer with a 2D GADDS detector. All X-ray photoelectron spectroscopy (XPS) peaks were referenced to the carbon C−(C, H) peak at 284.8 eV, and the data were obtained using a Physical Electronics PHI-5500 with charge neutralization. The room-temperature resistivity measurements were recorded on a Jandel four-point universal probe head combined with a Jandel resistivity unit. The equations used for calculating the resistivity were as follows: for pellets of <0.1 mm thickness, $\rho = [(\pi/\log n^2)(V/I)]t$, and, for pellets of >0.5 mm thickness, $\rho = 2\pi(S)(V/I)$, where ρ = resistivity, $\pi/(\log n^2)$ = sheet resistivity, V = voltage, I = current, t = thickness of the pellet, and S = the spacing of the probes (0.1 cm). Variable-temperature (VT) conductivity and magnetic measurements were conducted on a Quantum Design superconducting quantum interference device (SQUID) magnetometer MPMS system with a 5 T magnet from 4 to 200 K. Four copper wires were affixed to pressed pellets of the mesoporous composites with THF-solvated silver paste and then coated with a layer of epoxy for protection from the air. Raman spectra were recorded on a Renishaw Ramascope using a Renishaw 514 nm diode laser system.

Solid-state ^{87}Rb and ^{13}C NMR experiments were conducted on a Varian Infinity Plus 9.4 T wide-bore NMR spectrometer operating at $\upsilon_0(^{87}\text{Rb}) = 130.81$ MHz and $\upsilon_0(^{13}\text{C}) = 100.52$ MHz, using a Varian/Chemagnetics 4 mm HX MAS probe (operating in single-resonance ^{87}Rb or double-resonance ^{1}H−^{13}C configurations). NMR experiments were conducted on pristine Rb_3C_{60}, as well as a series of composite materials, including mesoporous tantalum oxide impregnated with Rb_3C_{60} (parent composite, $n = 1.0$), mesoporous tantalum oxide reduced with rubidium naphthalene only (1eq.Rb−TaTMSl), and parent composite materials reduced to the oxidation states of $n = 3.0$ and $n = 4.0$. Samples were ground into fine powders under a nitrogen atmosphere and tightly packed into zirconium oxide rotors, which were sealed at both ends by airtight Teflon caps and spacers.

Rubidium chemical shifts were referenced to 1.0 M $RbNO_3$ solution ($\delta_{iso}(^{87}\text{Rb}) = 0$ ppm). For both solid-state ^{87}Rb static and magic-angle spinning (MAS) NMR experiments, a spin−echo pulse sequence of the form $(\pi/2)_x-\tau_1-(\pi)_y-\tau_2-$acquire was applied (where τ_1 and τ_2 are the interpulse delays). The central transition selective $\pi/2$ pulse widths ranged from 1.45 to 4.0 μs, with rf fields ranging from $\upsilon_1 = 42.7$ kHz to $\upsilon_1 = 85.9$ kHz. Interpulse delays ranged from 35 to 100 μs for static echo experiments. For MAS experiments, samples were spun at $\upsilon_{rot} = 7-12.7$ kHz, and spin−echo experiments were rotor-synchronized. Recycle times for all samples were calibrated to 0.5 s or less, with the exception of the pure Rb_3C_{60} sample, for which a recycle time of 2 s was utilized. Between 20000 and 400000 transients were acquired for all static NMR experiments. The number of transients acquired for MAS NMR experiments ranged from ca. 320 to 17000, and from ca. 10900 to 22600 for SATRAS NMR experiments[26] in which the entire satellite transition manifold was acquired. Variable-temperature NMR experiments were performed on $n = 3.0$ and $n = 4.0$ composites over a temperature range of −120 to +25 °C for the former and from −120 to +100 °C for the latter.

Carbon chemical shifts were referenced to TMS ($\delta_{iso}(^{13}\text{C}) = 0$ ppm) by setting the high-frequency resonance of solid adamantane to 38.57 ppm. Solid-state ^{13}C{^{1}H} MAS NMR experiments were conducted on all samples with high-power continuous-wave proton decoupling ($\upsilon_2(^{1}\text{H}) = 35-58$ kHz) where appropriate. The $\pi/2$ pulse widths ranged from ca. 3.38 to 4 μs ($\upsilon_1(^{13}\text{C}) = 62.50-74.03$ kHz). The recycle times were calibrated between 9 and 40 s, and the number of collected transients ranged from ca. 544 to 8400. ^{13}C{^{1}H} VACP/MAS NMR experiments were performed only on samples with $n = 1.0$ and $n = 3.0$ and 1eq.Rb−TaTMSl, using ^{1}H $\pi/2$ pulse widths of 4 μs ($\upsilon_2(^{1}\text{H}) = 58.14$ kHz), calibrated recycle times between 6 and 10 s, and optimized contact times from 2 to 4 ms, and involved the collection of approximately 532−6500 transients.

All elemental analysis data were collected under an inert atmosphere by Galbraith Laboratories, 2323 Sycamore Dr., Knoxville, TN 37921-1700. Metal analysis was conducted by inductively coupled plasma (ICP) techniques.

(23) Lof, R. W.; van Veenendaal, M. A.; Koopmans, B.; Jonkman, H. T.; Sawatzky, G. A. *Phys. Rev. Lett.* **1992**, *68*, 3924.
(24) Durand, P.; Darling, G. R.; Dubitsky, Y.; Zaopo, A.; Rosseinsky, M. J. *Nat. Mater.* **2003**, *2*, 605.
(25) Skadtchenko, B. O.; Trudeau, M.; Kwon, C.-W.; Dunn, B.; Antonelli, D. M. *Chem. Mater.* **2004**, *16*, 2886.
(26) Jager, C.; Mullerwarmuth, W.; Mundus, C.; Vanwullen, L. *J. Non-Cryst. Solids* **1992**, *149*, 209.

Synthesis. Rb_3C_{60} was synthesized by heating a stoichiometric amount of C_{60} and Rb metal together in a vacuum-sealed tube at 400−450 °C for two months with periodic regrinding to ensure the homogeneity of the material, and was then characterized by Raman and XRD to ensure sample quality before proceeding with synthesis of the composite materials. The composites were synthesized as follows: an excess of Rb_3C_{60} was added to a suspension of mesoporous tantalum oxide in dry THF. The mesoporous solid immediately changed in color from light faun to deep gray-brown. After several days of additional stirring to ensure complete absorption of the fulleride, the reduced material was collected by suction filtration and washed several times with THF. Once synthesized, the material was dried in vacuo at 10^{-3} Torr on a Schlenk line until all condensable volatiles had been removed. Further reduction of these materials was accomplished by addition of a predetermined quantity (calculated on the basis of percent C in the material, corrected for C due to TMS groups) of a stock solution of rubidium naphthalene in THF to a stirred solution of the composite in THF. After being stirred overnight, the material was collected by suction filtration and washed several times with benzene until the washings were colorless. The material was then dried in vacuo at 10^{-3} Torr on a Schlenk line until all condensable volatiles had been removed. All materials were characterized by Raman, XPS, and elemental analysis to ensure sample quality before proceeding with SQUID and solid-state NMR studies. Room-temperature electron transport studies were conducted in triplicate in an inert atmosphere, allowing the system to stabilize for 30 min for each reading to ensure reproducibility. From the elemental analysis data on composites with fulleride oxidation states of n = 1.0, 3.0, and 4.0, molecular weights of 512.38, 590.73, and 602.93, respectively, normalized with respect to 1 mol of Ta, were calculated.

Results

Characterization and Electronic Properties. Treatment of a sample of mesoporous tantalum oxide with an excess of Rb_3C_{60} in THF over two weeks, until the maximum absorption of Rb_3C_{60} was reached, provided new dark brown powder (parent material). The BET (Brunauer, Emmett, Teller) surface area of this material dropped to 228 m^2/g as compared with 483 m^2/g in starting material, whereas the HK (Horvath−Kawazoe) pore size decreased from 22 to 19 Å. The loss of surface area and slight decrease in pore size in mesoporous transition-metal oxides upon absorption of large molecules is consistent with our previous results.[15,17,27,28] The nitrogen adsorption/desorption isotherm (Figure 1) was virtually the same as that of the starting material except for a small hysteresis in the parent material which may be due to the fulleride units causing a bottleneck effect in the pores. The X-ray powder diffraction pattern (Figure 2b) revealed a single peak falling at ca. d = 32 Å, similar to that of pure mesoporous tantalum oxide (Figure 2a). The elemental analysis of this powder gave values of 32.39% C as compared to 3.36% C in the starting material (Table 1). These data are consistent with adsorption of the fulleride from THF solution and partial occlusion of Rb_3C_{60} in the pores of the mesostructure. The Raman spectra (Figure 3a) of this new material showed a fulleride A_g peak at 1459 cm^{-1}, indicating an oxidation state of fulleride of n = 1.0, which is different from those of potassium/sodium fulleride systems studied previously.[15,17] The shift of the A_g band to the region of lower wavenumbers is likely due to the stronger reduction potential of Rb as compared with Na and K analogues. The X-ray photoelectron spectrum of this material is shown in Figure 4b and displays Ta 4f 7/2 and 5/2 emissions at 26.4 and 28.3 eV, respectively, as compared with 26.9 and 28.7 eV in pure mesoporous tantalum oxide (Figure 4a). The broad emissions in this region are due to the presence of more than one Ta species in the walls of the structure. For the sake of comparison, mesoporous tantalum oxide reduced with 1 equiv of rubidium naphthalene in the absence of C_{60} (1eq.Rb−TaTMSl) was prepared. The XRD pattern of this material indicated complete retention of the mesostructure (Figure 2e), while its XPS spectrum shown in Figure 4e

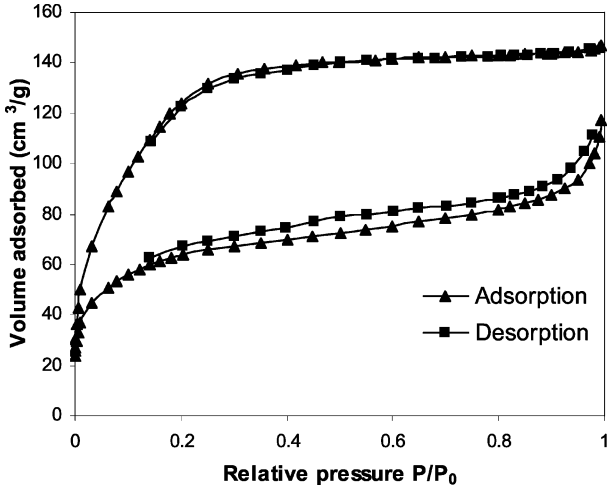

Figure 1. Nitrogen adsorption−desorption isotherms of mesoporous tantalum oxide before (upper) and after (lower) treatment with Rb_3C_{60}.

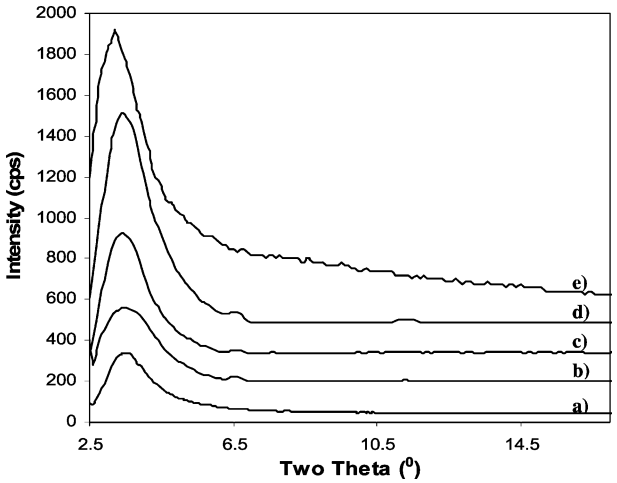

Figure 2. XRD spectra of (a) mesoporous tantalum oxide treated with trimethylsilane, (b) mesoporous tantalum oxide Rb_3C_{60} composite, (c, d) materials reduced to oxidation states of (c) n = 3.0 and (d) n = 4.0, and (e) mesoporous tantalum oxide reduced with 1 equiv of rubidium naphthalene in the absence of C_{60}.

Table 1. Table of Elemental Analysis Values for Samples of Mesoporous Tantalum Oxide Intercalated with Rubidium Fulleride at Various Levels of Reduction

sample ID	% C	% Ta	% Rb	molar ratio (C:Rb:Ta)
n = 1.0	32.39	35.28	21.7	13.85:1.3:1
n = 3.0	24.89	30.64	25.54	12.25:1.77:1
n = 4.0	17.97	30.02	26.95	9.03:1.91:1

(27) Hu, X.; Trudeau, M.; Antonelli, D. M. *Chem. Mater.* **2001**, *13*, 4808.
(28) He, X.; Trudeau, M.; Antonelli, D. M. *Chem. Mater.* **2001**, *13*, 4808.

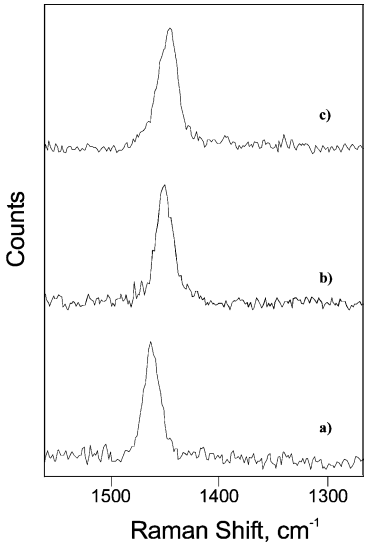

Figure 3. Raman spectra of (a) mesoporous tantalum oxide Rb_3C_{60} composite and (c, d) materials reduced to oxidation states of (b) $n = 3.0$ and (c) $n = 4.0$.

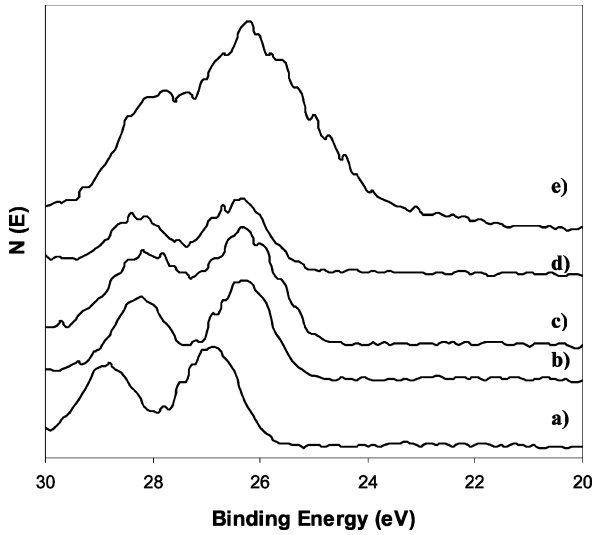

Figure 4. XPS spectra of samples from Figure 2 showing Ta 4f 7/2 and 5/2 regions.

revealed extremely broad Ta 4f 7/2 and 5/2 emissions at ca. 26.3 and 27.9 eV, respectively. Because these emissions are very broad and most likely correspond to the presence of mixed oxidation states, it is difficult to estimate the exact oxidation state of the mesoporous Ta framework, which roughly falls between +4.7 and +4.3.

The region near the Fermi level for the parent material is shown in Figure 5b, and that of pristine mesoporous tantalum oxide in Figure 5a. The spectrum of the composite exhibits one broad emission band tailing off at 4.0 eV for the O 2p valence band similar to other intercalate systems studied before. In the case of 1eq.Rb−TaTMSl the emission near the Fermi level is even broader (Figure 5e), tailing off at around 2.6 eV, indicating an increase in the density of states, yet the room-temperature conductivity measurements yield values of less than 10^{-7} Ω^{-1} cm^{-1}. The lack of any discernible peak for the Ta 5d level is typical of reduced mesoporous transition-metal oxides, where the amorphous nature of the walls leads to a broadened distribution of electronic states.[29] Furthermore, lifetime broadening near the

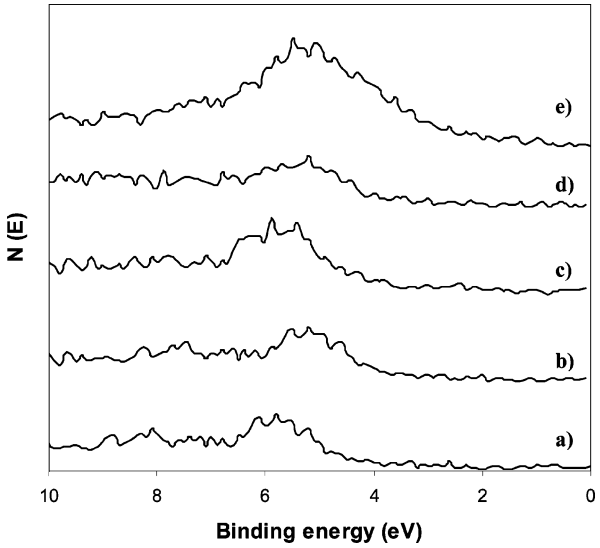

Figure 5. XPS spectra of samples from Figure 2 showing the region near the Fermi level.

Fermi level is common even in materials with highly crystalline structures, such as pristine mesoporous tantalum oxide.[30]

To explore the effect of the Rb loading level and the oxidation state of fulleride in the composite on conductivity, a series of composite materials was prepared by gradual titration of parent material with small amounts of rubidium naphthalene from a stock solution of known molarity, calculated on the basis of percent C in the parent material. The change in oxidation state of the fulleride units was monitored by Raman spectroscopy. It is well-known that for fulleride salts of the type A_nC_{60} (A = K, Rb, Cs) the A_g mode shifts roughly 6 cm^{-1} for every integer increment in the value of n.[31,32] Selected Raman spectra for the parent material and $n = 3.0$ and $n = 4.0$ composites are shown in Figure 3b, c. All further reduced composites retained their mesostructure as judged from the XRD patterns (Figure 2). The source of an additional bump at around 6.5 Å in the XRD spectra of all fulleride composites of mesoporous tantalum oxide is unknown, but it may be due to the presence of a small amount of a second phase. The XPS spectra of the Ta 4f 7/2 and 5/2 regions for the $n = 3.0$ and $n = 4.0$ materials are shown in parts c and d, respectively, of Figure 4, and indicate that no further reduction of the walls of the mesostructure has occurred on addition of rubidium naphthalene; however, substantial peak broadening indicative of the presence of mixed oxidation states is observed. The valence region near the Fermi level for the $n = 3.0$ and $n = 4.0$ materials is shown in parts c and d, respectively, of Figure 5, and displays a broad hump for the O 2p emission tailing off at about 4.0 eV for the $n = 3.0$ material, and at ca. 3.0 eV for the $n = 4.0$ material. The increased density of states near the Fermi level in the $n = 4.0$ material suggests an

(29) Vettraino, M.; Trudeau, M.; Antonelli, D. M. *Inorg. Chem.* **2001**, *40*, 2088.
(30) Cheetham, A. R.; Day, P. *Solid State Chemistry Techniques*; Oxford University Press: Oxford, 1998.
(31) Winter, J.; Kuzmany, H. *Solid State Commun.* **1992**, *84*, 935.
(32) Kuzmany, H.; Matus, M.; Burger, B.; Winter, J. *Adv. Mater.* **1994**, *6*, 731.

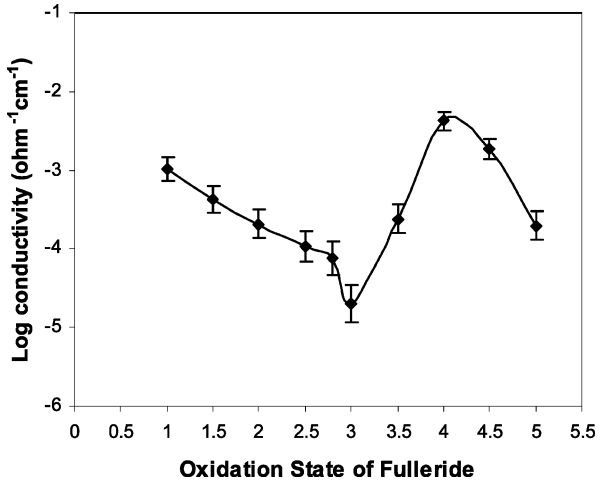

Figure 6. Logarithm of conductivity versus the oxidation state of fulleride at room temperature.

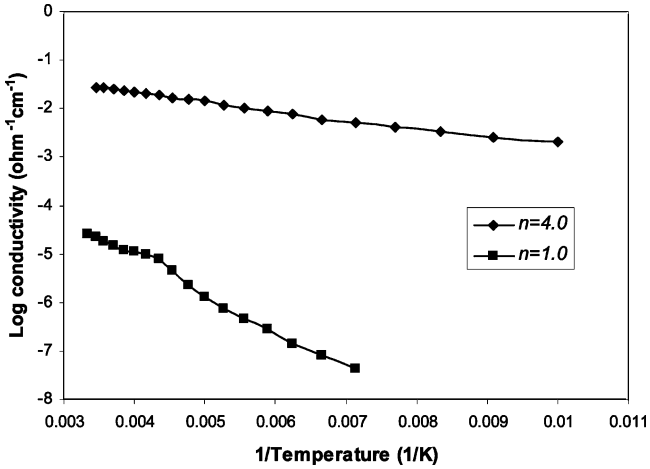

Figure 7. Logarithm of conductivity vs $1/T$ for $n = 1.0$ and $n = 4.0$ samples.

increase in conductivity of this material, as electron transport in bulk fullerides is closely related to the density of states near the Fermi level.[29] This is similar to what was observed for $n = 4.0-4.5$ potassium and sodium fulleride composites studied previously by our group, and was attributed to an increase in cooperative behavior between the conduction band of the mesostructure and the fulleride t_{1u} band.[15,17]

Figure 6 shows a plot of the logarithm of conductivity at room temperature versus the oxidation state of fullerene and exhibits a single maximum at $n = 4.0$. This pattern is in contrast with those for K_3C_{60} intercalates of mesoporous niobium, tantalum, and titanium oxides, where double maxima at $n = 2.5$ and $n \approx 4.0$ were observed,[15] but similar to that of the Na/Ta system, where a single conductivity maximum at $n = 4.5$ was noted.[17] The reason for the lack of a maximum between $n = 2.0$ and $n = 3.0$ is not understood, but may be due to the different electronic properties of rubidium/sodium fullerides and potassium fullerides.

Since room-temperature conductivity measurements provide only a limited amount of information on the electronic properties of a material, variable-temperature conductivity measurements were employed for the samples with $n = 1.0$ and $n = 4.0$. The other materials in this study were too insulating to provide meaningful voltage readings over a broad temperature range. Figure 7 shows a plot of the logarithm of conductivity versus $1/T$. The $n = 1.0$ composite behaves as a semiconductor down to 230 K, below which a transition to a more insulating state occurs. These types of transitions are typical for one-dimensional materials and are normally attributed to Peierls distortion and charge density waves resulting in electron localization.[30] The $n = 4.0$ material, on the other hand, behaves more like a semimetal or a narrow band gap semiconductor with a small elbow at around 150 K.

Table 1 summarizes the C:Ta:Na ratios of the materials for $n = 1.0$, $n = 3.0$, and $n = 4.0$. The percent C analysis of these materials shows that the carbon loading level gradually drops as more Rb is introduced into the system. This trend is consistent with K_3C_{60} intercalates, which show a general decrease in carbon loading from ca. 30% to ca. 10% as the fulleride is gradually reduced to $n = 3.0$. The progressive leaching of fulleride from the channels of the mesostructure from $n = 0.5$ to $n = 3.0$ was explained previously[15] by an increase in Coulombic repulsion between the fulleride units with increasing potassium loading level, essentially pushing fulleride out of the pores, as well as the higher solubility of $n = 3.0$ fullerides in THF as compared to less reduced species.[15] The observation of gradual carbon leaching at a higher level of reduction is important as it further supports our hypothesis that conductivity in these composite materials does not depend as strongly on the absolute carbon level as it does on the oxidation state of the fulleride.[17]

SQUID magnetometer measurements over the temperature range 4−200 K at 500 G were performed for $n = 1.0$, 3.0, and 4.0 materials and are shown in Figure 8. The plot of magnetic susceptibility (χ) vs T (Figure 8a) indicates that all the materials are paramagnetic and possess both free-spin Langevin and temperature-independent (Van Vleck) paramagnetism. The plot χ vs $1/T$ shown in Figure 8b demonstrates that these materials strictly obey the Curie law from 4 to 200 K with the Curie constants shown in Table 2. The absolute values of the magnetic moments for these materials were calculated and showed a substantial increase as more rubidium was introduced into the pores, corresponding to an increase in unpaired electrons in the system, which could have some pairing with Ta−Ta bonds on the walls of the mesostructure as proposed previously for alkali-metal-reduced mesoporous niobium oxide.[29] Table 2 also lists the temperature-independent terms. The increasing magnitude of these values parallels the increasing conductivity, suggesting that some of the temperature-independent paramagnetism may be due to Pauli paramagnetism, at least in the $n = 4.0$ sample. Pauli paramagnetism is normally associated with metallic behaviors; however, it is usually much smaller in magnitude than Van Vleck paramagnetism.

Solid-State ^{87}Rb and ^{13}C NMR Studies. To gain further insight into the coordination and structural geometry of fulleride in rubidium fulleride composites, solid-state ^{87}Rb and ^{13}C NMR measurements were carried out. In our previous NMR investigations of mesoporous tantalum oxide sodium fulleride composites, it was found that it is possible to distinguish various types of sodium species via straightforward ^{23}Na magic-angle spinning (MAS) NMR experi-

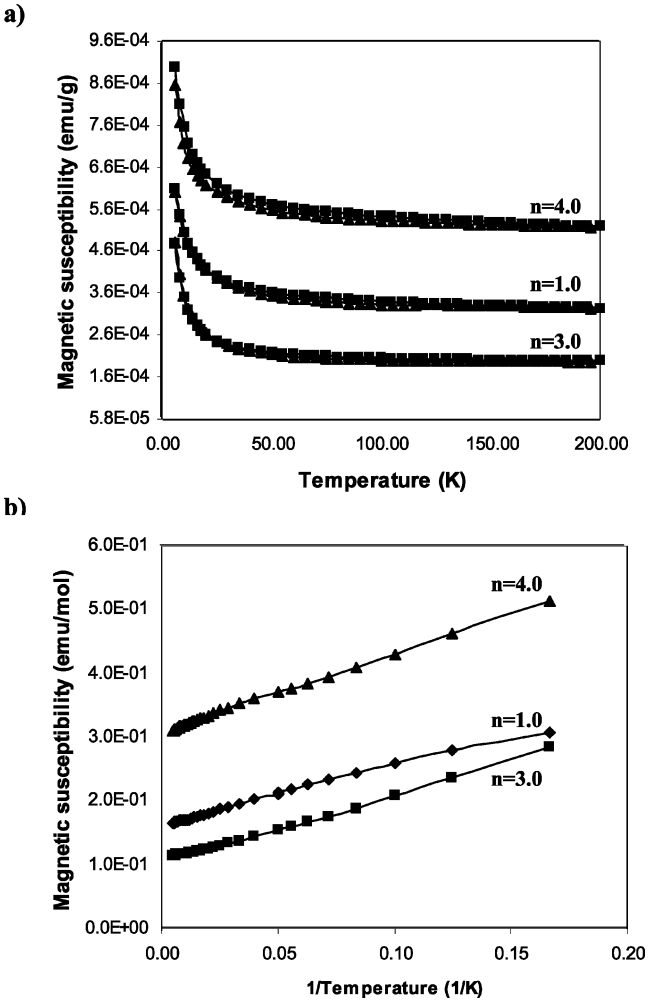

Figure 8. (a) Magnetic susceptibility versus temperature and (b) normalized molar magnetic susceptibility versus inverse temperature of samples from Figure 3.

Table 2. Table of the Temperature-Independent Paramagnetic Term, Curie Constant, and Effective Magnetic Moment (μ_{eff}) from Table 1

sample ID	temperature-independent paramagnetic term (emu/mol)	Curie constant [(emu K)/mol]	μ_{eff} (μ_B)
$n = 1.0$	0.162	0.82	0.78
$n = 3.0$	0.107	1.1	0.91
$n = 4.0$	0.307	1.23	0.95

ments.[17] Three different types of sodium sites were differentiated, including sodium ions in the mesoporous channels, sodium ions confined in the tantalum oxide framework, and sodium ions that are associated with the different species of fullerides. ^{87}Rb, like ^{23}Na, is a half-integer quadrupolar nucleus (nuclear spin $I = 3/2$), and is very amenable to NMR experimentation due to its high receptivity and relatively small nuclear quadrupole moment ($Q = 0.1335 \times 10^{-27}$ m^2).[33] ^{85}Rb is the other NMR-active isotope of rubidium, is 0.15 times as receptive as ^{87}Rb, and also has a nuclear quadrupole moment which is roughly twice that of ^{87}Rb. ^{87}Rb NMR has proven to be an invaluable probe of the structure of alkali-metal fullerides,[34,35] and has also been used to probe Rb ion environments in a variety of materials, including Rb salts intercalated into γ-alumina,[36] Rb ions in halide lattices,[37] Rb^- ions in zeolite LiA,[38] and rubidium cations in various sites in zeolites NH_4Y and LTA.[39,40] As for the sodium fullerides encapsulated into mesoporous metal oxides, or rubidium sites in microporous solids, the different chemical environments of the alkali-metal species in mesoporous metal oxides should induce quadrupolar and chemical shielding interactions which can be employed to build an understanding of the molecular structure and dynamics in these composite materials. The rubidium chemical shift range is considerably larger than that of sodium,[41] so it is possible that additional species which could not be identified by ^{23}Na NMR experiments will be observed in the ^{87}Rb NMR spectra. Additionally, $^{13}C\{^1H\}$ MAS and $^{13}C\{^1H\}$ VACP/MAS (variable-amplitude cross polarization) experiments were employed to identify the carbon-containing species in these composite materials, as well as to monitor changes in the oxidation states of the fullerene and fulleride species. Before proceeding with the discussion on NMR data of our composites, it is prudent to review solid-state NMR data for pristine Rb_3C_{60}.

Solid-State ^{87}Rb and ^{13}C NMR of Rb_3C_{60}. Much effort has been expended on the structural characterization of alkali-metal fullerides, due to the high-temperature superconductivity observed in alkali-metal fullerides of the form A_3C_{60}, which has been surpassed only by high T_c copper oxides.[42] Rb_3C_{60} has been the subject of numerous solid-state NMR investigations.[34,35] An initial paper on the synthesis and structural characterization of alkali-metal fullerides proposed that Rb_3C_{60} may have a structure with tetrahedral (T) and octahedral (O) sites.[42] Tetrahedral and octahedral coordination sites in these alkali-metal fullerides refer to alkali-metal cations coordinated to 24 and 12 carbon atoms from the neighboring fulleride species, respectively. Tycko et al. used ^{13}C NMR to investigate Rb_3C_{60} and other alkali-metal fullerides.[43,44] Static ^{13}C NMR experiments at ambient temperature revealed a broad anisotropic pattern with a center of gravity near 181 ppm,[43] whereas slow-spinning (3.5 kHz) MAS NMR spectra show an isotropic peak near 197 ppm, corresponding to the C_{60}^{3-} species, and a less intense resonance at 191 ppm, which is thought to arise from a Rb_4C_{60} impurity phase.[44] Pennington and Stenger claim to observe the isotropic peak for C_{60}^{3-} nearer to 182 ppm.[34] The broad peaks in the ^{13}C MAS NMR spectrum of Rb_3C_{60} are thought to arise from structural disorder, which gives rise to an inhomogeneous distribution of chemical shifts.

(33) Pyykkö, P. *Mol. Phys.* **2001**, *99*, 1617.
(34) Pennington, C. H.; Stenger, V. A. *Rev. Mod. Phys.* **1996**, *68*, 855.
(35) Rosseinsky, M. J. *Chem. Mater.* **1998**, *10*, 2665.
(36) Cheng, J. T.; Ellis, P. D. *J. Phys. Chem.* **1989**, *93*, 2549.
(37) de Dios, A. C.; Walling, A.; Cameron, I.; Ratcliffe, C. I.; Ripmeester, J. A. *J. Phys. Chem. A* **2000**, *104*, 908.
(38) Terskikh, V. V.; Lapina, O. B.; Bondareva, V. M. *Phys. Chem. Chem. Phys.* **2000**, *2*, 2441.
(39) Ciraolo, M. F.; Hanson, J. C.; Grey, C. P. *Microporous Mesoporous Mater.* **2001**, *49*, 111.
(40) Igarashi, M.; Kodaira, T.; Ikeda, T.; Itoh, M.; Shimizu, T.; Goto, A.; Nozue, Y. *Physica B: Condens. Matter* **2003**, *327*, 72.
(41) Mason, J. *Multinuclear NMR*; Plenum Press: New York, 1987.
(42) Murphy, D. W.; Rosseinsky, M. J.; Fleming, R. M.; Tycko, R.; Ramirez, A. P.; Haddon, R. C.; Siegrist, T.; Dabbagh, G.; Tully, J. C.; Walstedt, R. E. *J. Phys. Chem. Solids* **1992**, *53*, 1321.
(43) Tycko, R.; Dabbagh, G.; Rosseinsky, M. J.; Murphy, D. W.; Ramirez, A. P.; Fleming, R. M. *Phys. Rev. Lett.* **1992**, *68*, 1912.
(44) Tycko, R. *J. Phys. Chem. Solids* **1993**, *54*, 1713.

^{87}Rb NMR spectra acquired at 440 K show that there are T and O rubidium sites in a 2:1 ratio.[45,46] As the temperature is dropped below 370 K, there is an additional resonance which is attributed to a second type of tetrahedral Rb site (T′). SEDOR NMR experiments imply that all three sites originate within the same phase.[45] It was suggested that the T′ site may arise from unique orientations or differential motion of the C_{60} molecules at lower temperatures (i.e., which deviate from the fcc structure of Rb_3C_{60}),[45,46] Jahn−Teller distortion of the C_{60}^{3-} molecules, or even localization of excess charge density at the T′ sites, though most of these claims were disproved.[47] Later ^{87}Rb NMR studies by Zimmer et al. revealed fine structural detail in MAS NMR experiments not observed in previous static NMR experiments,[48] and 2D chemical exchange spectra showed no exchange between the various Rb sites.[49] The authors suggested that diffusion of Rb atoms between vacancies is a possible explanation for differentiation of the T and T′ sites in the ^{87}Rb spectra, though this was later shown not to be the case by Gorny et al.,[50] who suggested that the differences in the T and T′ sites likely arise from variations in the surroundings.

Our own ^{87}Rb static NMR experiments on Rb_3C_{60} reveal three relatively broad powder patterns centered at 80, −11, and −135 ppm (Figure 9a), in agreement with previously acquired NMR data.[45−47,51] The centers of gravity of these patterns are assigned to the Rb ions in T′, T, and O sites, respectively. ^{87}Rb MAS NMR experiments serve to narrow the broad patterns substantially (Figure 9b), revealing some second-order structure in the two lower frequency patterns, with centers of gravity at 80, 2.2, and −123 ppm. The corresponding ^{13}C{^{1}H} MAS NMR spectra (Figure 9c, d) have a sharp peak centered at 182.8 ppm as well as a broad nonuniform peak near 195 ppm. The former is assigned to the C_{60}^{3-} species,[34] while the latter may reflect a distribution of chemical shifts arising from some disorder in the sample, or from other nonstoichiometric rubidium fulleride species similar to that observed in Na_3C_{60} composites.[15] There are also some relatively weak signals at 144 and 111 ppm, which are assigned to unreacted C_{60}[52] and Teflon contained within the sample spacers,[53] respectively.

Solid-State ^{87}Rb and ^{13}C NMR of Rb Composites. To make more direct comparisons between the bulk phase of Rb_3C_{60} and mesoporous composite materials, and to elucidate the effect of coordination geometries of both the fulleride and rubidium species on the unusual electronic properties of the composite materials, solid-state ^{87}Rb and ^{13}C NMR measurements were employed for the samples with $n = 1.0$, $n = 3.0$, and $n = 4.0$ as well as for 1eq.Rb−TaTMSl, which is C_{60}^- "free".

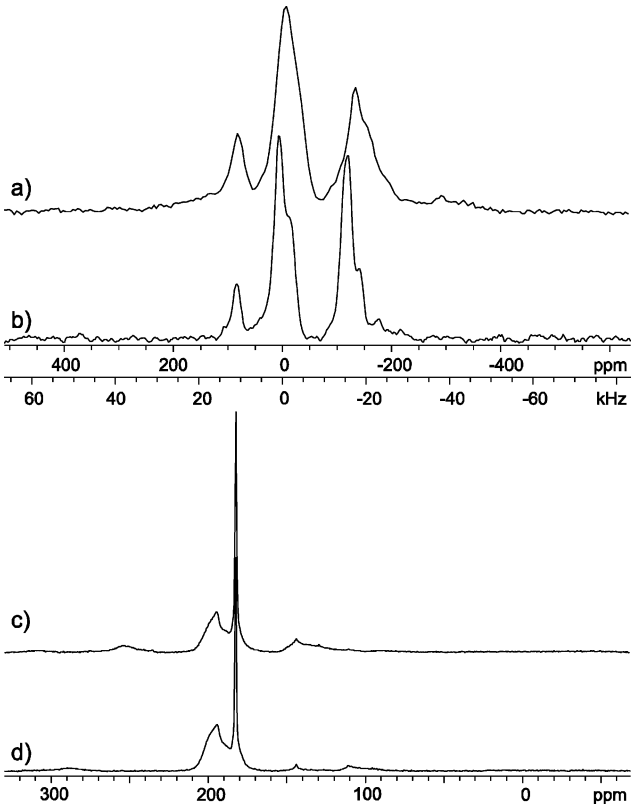

Figure 9. (a) ^{87}Rb static NMR spectrum and (b) ^{87}Rb MAS NMR spectrum ($\nu_{rot} = 12$ kHz) of Rb_3C_{60} at 9.4 T. ^{13}C MAS NMR spectra of Rb_3C_{60} at (c) $\nu_{rot} = 5.3$ kHz and (d) $\nu_{rot} = 8.7$ kHz.

The room-temperature ^{87}Rb MAS NMR spectrum of 1eq.Rb−TaTMSl (Figure 10a) possesses a major resonance at 130 ppm, as well as two other minor resonances at 119 ppm (sharp) and 65 ppm (broad). There is also an extremely broad powder pattern which spans ca. 350 kHz (see the inset of Figure 10a), underlying the main peak and spinning sidebands. The major resonance at 130 ppm corresponds to Rb ions in the channel of the mesostructure. The origin of peaks at 119 and 0 ppm is not known for certain, but is likely related to unique Rb environments in the channels, or perhaps in smaller microporous channels. Peaks such as these were not observed in analogous ^{23}Na NMR experiments on tantalum oxide reduced with sodium naphthalene,[17] because the sites either simply did not exist or were not resolved in the reduced sodium chemical shift range (i.e., sites may have had overlapping resonances). These peaks may also be due to formation of the rubidium tantalate phase due to slight overreduction of the framework, as they are not present in a sample of mesoporous tantalum oxide reduced with only 0.5 equiv of rubidium naphthalene. Previous work in our group demonstrated that treatment of mesoporous titanium oxide with more than 1.0 equiv of lithium naphthalene reagent led to destruction of the mesostructure and formation of numerous lithium titanate phases.[29]

The broad underlying pattern likely arises from the presence of Rb ions which are confined within the metal oxide framework (i.e., Rb ions which are strongly interacting

(45) Walstedt, R. E.; Murphy, D. W.; Rosseinsky, M. J. *Nature* **1993**, *362*, 611.
(46) Buffinger, D. R.; Ziebarth, R. P.; Stenger, C. A.; Recchia, C.; Pennington, C. H. *J. Am. Chem. Soc.* **1993**, *115*, 9267.
(47) Pennington, C. H.; Hahm, C.; Stenger, V. A.; Gorny, K.; Recchia, C. H.; Martindale, J. A.; Buffinger, D. R.; Ziebarth, R. P. *Phys. Rev. B* **1996**, *54*, r6853.
(48) Zimmer, G.; Thier, K. F.; Mehring, M.; Rachdi, F.; Fischer, J. E. *Phys. Rev. B* **1996**, *53*, 5620.
(49) Zimmer, G.; Mehring, M.; Rachdi, F.; Fischer, J. E. *Phys. Rev. B* **1996**, *54*, R3768.
(50) Gorny, K.; Hahm, C.; Martindale, J. A.; Yu, S.; Pennington, C. H.; Buffinger, D. R.; Ziebarth, R. P. *Phys. Rev. Lett.* **1997**, *79*, 5118.
(51) Stenger, C. A.; Recchia, C.; Vance, J.; Pennington, C. H.; Buffinger, D. R.; Ziebarth, R. P. *Phys. Rev. B* **1993**, *48*, 9942.
(52) Tycko, R.; Dabbagh, G.; Rosseinsky, M. J.; Murphy, D. W.; Ramirez, A. P.; Fleming, R. M. *Phys. Rev. Lett.* **1992**, *68*, 1912.
(53) Liu, S. F.; Schmidt-Rohr, K. *Macromolecules* **2001**, *34*, 8416.

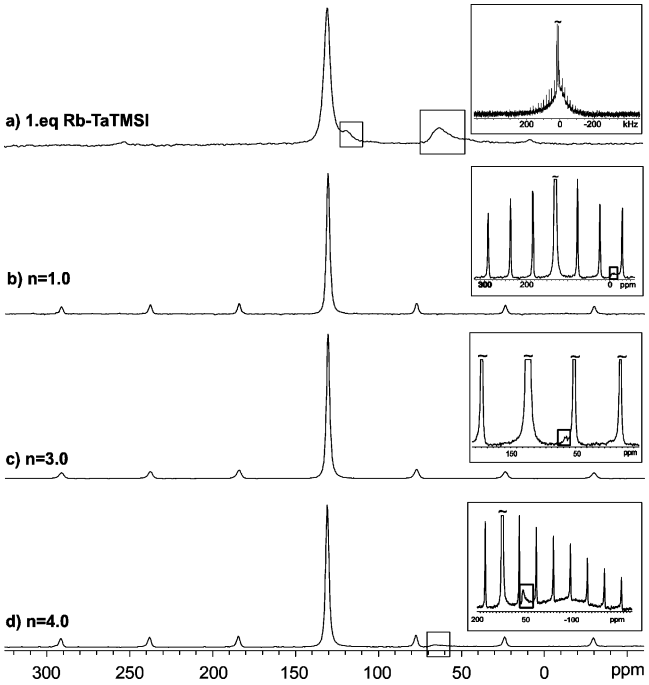

Figure 10. ^{87}Rb MAS NMR spectra of (a) mesoporous tantalum oxide reduced with rubidium naphthalene in the absence of C_{60}, (b) mesoporous tantalum oxide Rb_3C_{60} composite ($n = 1.0$), and (c, d) mesoporous tantalum oxide Rb_3C_{60} composite reduced to oxidation states of (c) $n = 3.0$ and (d) $n = 4.0$. Inset: Vertical expansions of isotropic chemical shift regions.

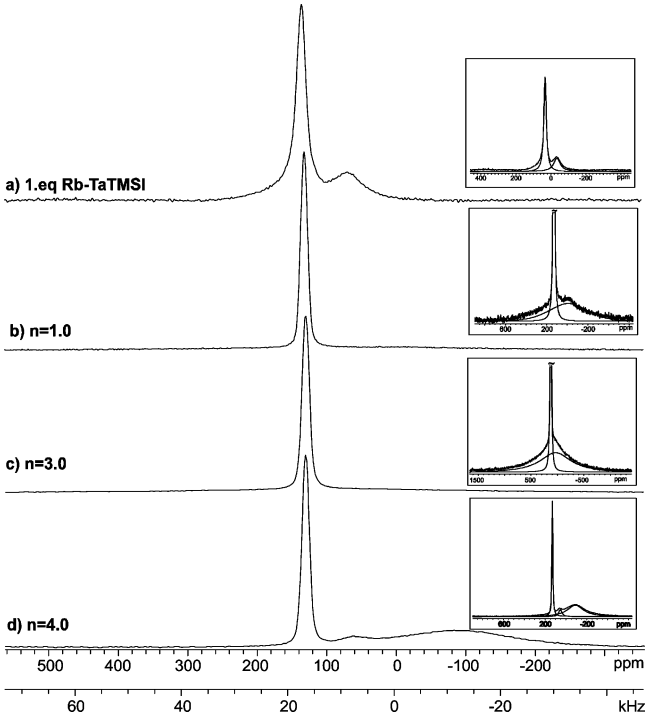

Figure 11. ^{87}Rb static NMR spectra of samples from Figure 10. Inset: Vertical expansions and deconvolution of peaks.

with oxygen atoms of the metal oxide framework and/or tightly bound surface species). This is consistent with the XPS spectrum which suggests substantial reduction of the tantalum oxide walls by rubidium naphthalene, and is further confirmed by static ^{87}Rb NMR spectra. Similar assignments have been made for ^{23}Na NMR spectra of Na ions resulting from the encapsulation of Na_3C_{60} into mesoporous tantalum oxide,[17] as well as "surface" and "buried" sodium sites in sodium-doped mesoporous aluminosilicates.[54]

The static ^{87}Rb NMR spectrum of 1eq.Rb−TaTMSl (Figure 11a) displays two main powder patterns. The resonances, observed in the MAS NMR spectrum, at 130 and 119 ppm overlap, giving rise to a single broad powder pattern with a center of gravity at 133 ppm and an fwhh of ca. 2.2 kHz, while the second powder pattern is centered at 65 ppm with an fwhh of ca. 6.3 kHz. The relative integrated areas of these powder patterns are 3:1 in favor of the higher frequency pattern. Thus, MAS and static ^{87}Rb NMR experiments identify two major rubidium sites: "channel" Rb ions and framework Rb ions, which give rise to an intense sharp resonance at ca. 133 ppm and a broad overlapping resonance at ca. 65 ppm, respectively.

The ^{13}C MAS and VACP/MAS NMR spectra of 1eq.Rb−TaTMSl revealed a wide variety of different resonances, including benzene (129 ppm), Teflon from the spacers of the rotor (112 ppm), THF (68 and 26 ppm), and some residual tetramethylsilyl chloride (near 0 ppm), as well as some other carbon-containing species with resonances at 73 and 56 ppm which may arise from coordination of THF by Rb ions (Figure 12a). The intense peak centered at ca. 128.5

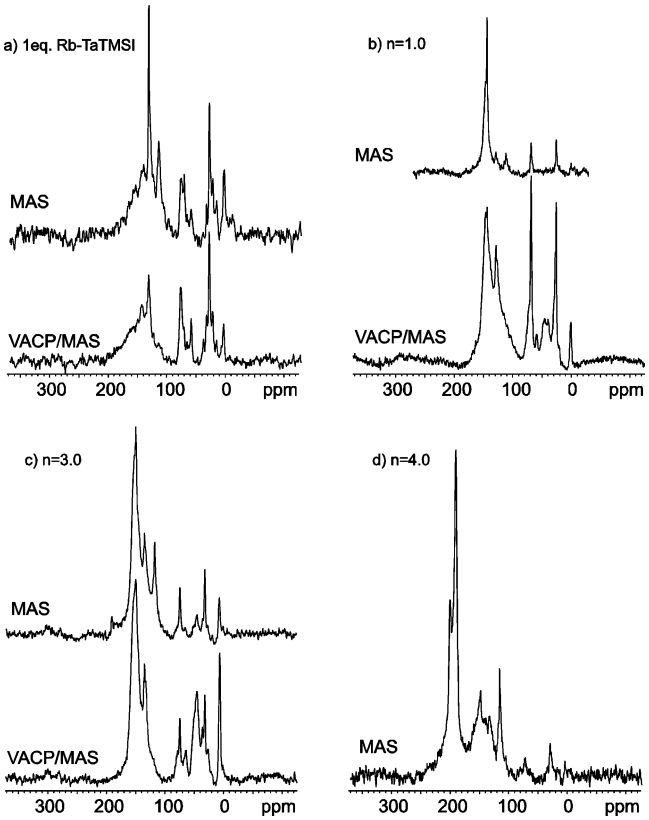

Figure 12. ^{13}C MAS NMR spectra ($\nu_{rot} = 15$ kHz) of samples from Figure 10. Corresponding ^{13}C VACP/MAS spectra are shown for all samples with the exception of the $n = 4.0$ sample.

ppm in the ^{13}C MAS spectrum of 1eq.Rb−TaTMSl arises from the overlap of benzene resonance ($\delta_{iso} = 128.5$ ppm) with the naphthalene resonances ($\delta_{iso} = 126.1$, 128.3, and 133.9 ppm).[55] There is a broad powder pattern that ranges

(54) Du, H. B.; Terskikh, V. V.; Ratcliffe, C. I.; Rimpmeester, J. A. *J. Am. Chem. Soc.* **2002**, *124*, 4216.

(55) Gunther, H. *NMR Spectroscopy*; John Wiley & Sons: New York, 1980.

from 100 to 200 ppm, which likely results from an inhomogeneous chemical shift distribution resulting from organic species interacting with the mesoporous channels and a variety of different environments within the metal oxide framework.

The ^{87}Rb MAS NMR spectrum of the parent ($n = 1.0$) material is shown in Figure 10b. There is one major sharp peak at 131 ppm flanked by a manifold of spinning sidebands (SSBs), as well as a much smaller resonance at ca. −8 ppm. The SSBs indicate that there is a sizable quadrupolar interaction, though not large enough to give rise to a second-order central transition powder pattern. Simulations of the isotropic resonance and SSBs using SIMPSON do not yield any precise quantitative information regarding the magnitude of the quadrupolar interaction (room-temperature ^{87}Rb SATRAS NMR spectrum not shown), since the SSBs taper off on each side of the central transition, probably as a result of long-range disorder in the solid. None of the ^{87}Rb NMR resonances observed for the pure phase Rb_3C_{60} are observed for this sample or for any of the other composite materials (vide infra). The small resonance at −8 ppm may correspond to Rb species associated with a fulleride species. Differing from the ^{87}Rb MAS NMR spectra of 1eq.Rb−TaTMSl, a broad underlying powder pattern is absent, implying less incorporation of Rb ions into the walls of the mesostructure in the parent material, which is consistent with the lower reduction level of the Ta framework.

In a vertical expansion of the ^{87}Rb static NMR spectrum of the $n = 1.0$ material, a broad underlying powder pattern centered at ca. -10 ± 10 ppm is observed (Figure 11b). The intense peak at 131 ppm corresponds to Rb cations in the channels of the mesoporous tantalum oxide, whereas the latter broad peak near −10 ppm may arise from the presence of one or more Rb species associated with fulleride units. The absence of visible resonances at around ca. 65 ppm is not surprising as this quite weak resonance is most likely obscured by rubidium fulleride species which are dominant in this case.

The ^{13}C MAS NMR spectrum of the $n = 1.0$ material (Figure 12b) has the same signature peaks as that of the 1eq.Rb−TaTMSl sample (i.e., benzene, Teflon, THF, and TMSl) as well as additional C_{60} and C_{60}^{n-} resonances. A sharp peak at 144 ppm and a neighboring broader peak centered at 148 ppm are also evident. The narrow resonance at 144 ppm likely corresponds to pure C_{60}, while the latter resonance corresponds to a fulleride species in a distinct oxidation state, C_{60}^{n-}; however, the assignment of the exact oxidation state of this species is not possible at this time. Interestingly, no trace of C_{60}^{3-} resonances is detected, further affirming that Rb_3C_{60} was oxidized by the channels of the metal oxide framework. In the ^{13}C VACP/MAS NMR spectra, the Teflon resonance completely disappears, the intensity of the C_{60} resonances becomes greatly reduced, and the benzene, THF, and TMSl peaks are enhanced, as anticipated. There are also broad unidentified peaks at ca. 59, 46, and 40 ppm.

The ^{87}Rb MAS NMR spectrum of the $n = 3.0$ material (Figure 10c) is almost identical to the spectrum of the parent material. The peaks correspond to Rb ions within the channel of the parent and $n = 3.0$ materials and have almost identical fwhh values of ca. 320 Hz. The only noticeable differences are (i) a very subtle peak near 65 ppm and (ii) the absence of a very small peak near −8 ppm. The spinning sideband manifold extends a similar distance as compared to the spectra of the parent material, indicating that the quadrupolar interactions are similar (not shown). The peak at 65 ppm (Figure 10c, inset) likely corresponds to framework Rb ions consistent with the peak at the same position in 1eq.Rb−TaTMSl, and the progressive reduction of the mesoporous tantalum oxide as evident from XPS measurements (Figure 4).

The static ^{87}Rb NMR spectrum of the $n = 3.0$ composite (Figure 11c) appears to be similar to that of the parent material. However, expansion of the vertical scale reveals a broad underlying pattern, distinct from that of the parent material, which extends in the high- and low-frequency directions. This pattern undoubtedly arises from overlapping powder patterns corresponding to both framework Rb ions and Rb ions associated with the various fulleride species. The degree of Rb ion incorporation into the framework is higher than in parent material, but clearly much lower than in the 1eq.Rb−TaTMSl sample.

The ^{13}C MAS and VACP/MAS NMR spectra of the $n = 3.0$ composite (Figure 12c) are very similar to those of the parent composite (Figure 12b). However, the ^{13}C NMR spectrum of the $n = 3.0$ material shows an increased amount of C_{60}^{n-} species and less C_{60} than in the parent material. In addition, there is a very small resonance at ca. 184 ppm which can be assigned to C_{60}^{3-}. These results are distinct from those of ^{13}C MAS NMR experiments previously conducted on mesoporous tantalum oxide impregnated with Na_3C_{60} and reduced with sodium naphthalene to the oxidation state of $n = 3.0$.[17] In these samples, the C_{60} species of the parent material were completely reduced to C_{60}^{3-} (i.e., a sharp peak at 187.3 ppm was the only indicator of fullerene/fulleride species) upon reduction, whereas in Rb samples reduced to the same oxidation state of $n = 3.0$ only a minute amount of C_{60}^{3-} is produced. The ^{87}Rb and ^{13}C NMR data therefore imply that $n = 1.0$ and $n = 3.0$ samples are very similar, with the exception of more confined Rb ions in the $n = 3.0$ material and the conversion of a small amount of C_{60} to C_{60}^{3-}. The near absence of C_{60}^{3-} is conspicuous, especially given that Raman spectra suggest a fulleride oxidation state of $n = 3.0$. These data collectively imply that the band at 1447 cm^{-1} in the Raman spectrum of this material arises from an averaging of signals from several contributing fulleride species and not, in fact, from C_{60}^{3-} itself. This observation is in keeping with previous work in our group which suggests that Raman spectroscopy alone is not a reliable method to assign fulleride oxidation states in a sample.

The ^{87}Rb MAS NMR spectrum of the $n = 4.0$ material appears to combine elements of all of the other composites (Figure 10d). The usual sharp channel Rb site is present as evidenced by a peak at 130 ppm. There is a pronounced resonance at 65 ppm, similar to that observed in the 1eq.Rb−TaTMSl and $n = 3.0$ samples which corresponds to confined Rb ions in the walls of the mesostructure. Finally, there is

also a very broad powder pattern centered at ca. −75 ppm. This pattern most likely corresponds to the Rb associated with one or more fulleride species.

The static ^{87}Rb NMR spectrum of the $n = 4.0$ composite (Figure 11d) is consistent with increased intercalation of Rb ions into the walls of the mesostructure relative to that of the $n = 1.0$ and $n = 3.0$ samples upon increased reduction to the $n = 4.0$ state. The reduction of the walls is also supported by XPS data (Figure 4). The resonance at −75 ppm, previously assigned to Rb associated with particular fulleride species, is also prominent. The relative integrated area of channel (130 ppm) to confined (65 ppm) to fulleride-related (−75 ppm) species is ca. 8:1:14, indicating the presence of the substantial amount of Rb ions associated with the new fulleride species in the channels identified in the ^{13}C NMR spectrum of this material.

Perhaps of equal interest is the ^{13}C MAS NMR spectrum of the $n = 4.0$ material (Figure 12d). There are major resonances at 186 and 196 ppm which can be assigned to C_{60}^{3-} and some other anionic C_{60}^{n-} species. The resonance near 144 ppm is greatly diminished in intensity, indicating that most of the C_{60} has been reduced to other fulleride species. These data further support the assumption that the broad powder pattern centered at −75 ppm observed in ^{87}-Rb MAS NMR is likely due to Rb ions coordinated to a fulleride species in the $n = 4.0$ sample as compared to the $n = 3.0$ sample, which has very little or no C_{60}^{3-} and showed a less intense peak at −75 ppm in static ^{87}Rb NMR. As equally intriguing is that it was not possible to conduct ^{13}C MAS (with high-power decoupling) or VACP/MAS NMR experiments, since it was impossible to obtain a reasonable matching/tuning combination on the proton channel for this sample. The inability to tune or match on the narrow-banded proton channel indicates that the $n = 4.0$ material has a significant influence on the inductance of the sample coil, likely because of the strong magnetic properties which distinguish this sample from all of the other materials. This is consistent with SQUID measurements, which revealed that the $n = 4.0$ sample possesses the greatest degree of temperature-independent paramagnetism.

Variable-Temperature ^{87}Rb NMR of Rubidium Fulleride Composites. Variable-temperature solid-state NMR is a very useful analytical tool widely applied to probe temperature-dependent motion in solids. The change of structure with temperature is closely related to metal−insulator transitions in one-dimensional solids, and for this reason variable-temperature studies of these materials may be useful in understanding their charge transport behavior. To this end variable-temperature ^{87}Rb NMR experiments were conducted on the most insulating ($n = 3.0$) and the most conducting ($n = 4.0$) composite materials. The ^{87}Rb resonances which are assigned to channel Rb ions in $n = 3.0$ and $n = 4.0$ samples shift to high frequency as the temperature is lowered (Figure 13). A similar temperature response is also observed for the smaller ^{87}Rb resonance near 65 ppm at room temperature of the $n = 4.0$ sample (Figure 14). Interestingly, an analogous temperature-dependent shift was not observed for the channel Na ions in the ^{23}Na NMR spectra in the Na/Ta system,[17] though the minor ^{23}Na

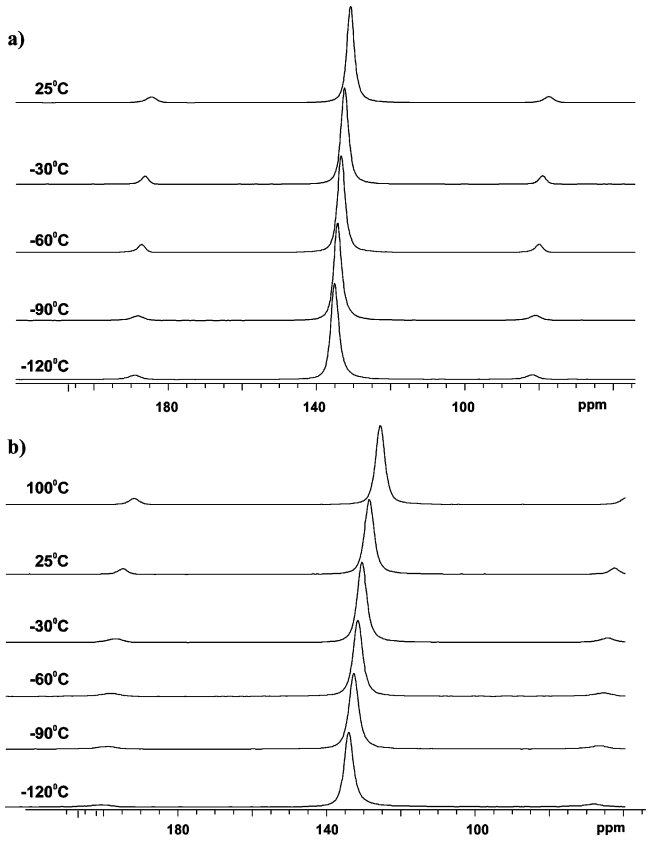

Figure 13. Variable-temperature ^{87}Rb MAS NMR spectra showing an expanded region containing an isotropic peak for (a) $n = 3.0$ and (b) $n = 4.0$ composites.

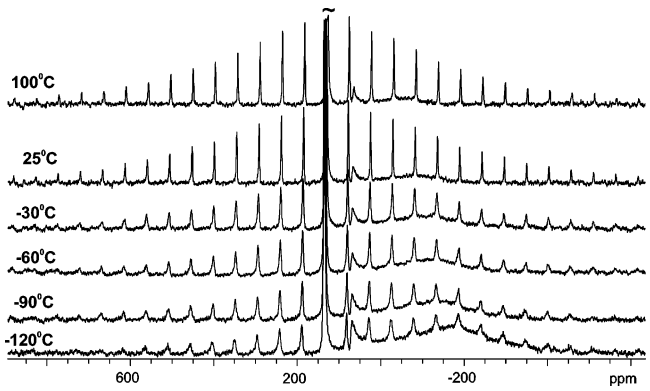

Figure 14. Variable-temperature ^{87}Rb MAS NMR spectra of the entire spinning sideband manifold for the $n = 4.0$ sample.

resonance of Na ions closely associated with fulleride species did exhibit similar high-frequency shifts with decreasing temperature. The broad powder pattern centered at −60 ppm at +100 °C (Figure 14) shifts in the low-frequency direction to −185 ppm at −120 °C. It is known that at lower temperatures the thermal motions in the solid are decreased, leading to a reduction in the motional averaging.[56,57] As a result, increases in the values of C_Q are typically observed with decreasing temperature, which results in a "quadrupolar-induced shift" of the center of gravity of the pattern to the low-frequency direction. Rb sites associated with fulleride

(56) Das, T. P.; Hahn, E. L. *Nuclear Quadrupole Resonance Spectroscopy*; Academic Press Inc.: New York, 1958.
(57) Lucken, E. A. C. *Nuclear Quadrupole Coupling Constants*; Academic Press: New York, 1969.

species which are extremely restricted in motion will be subject to such an effect, and should experience an increase in C_Q with decreasing temperature. It is also possible that a small temperature-dependent chemical shift, perhaps opposite that observed for the Rb species discussed above, may also contribute to the observed spectra. Such behavior has been observed in ^{87}Rb NMR spectra of a variety of inorganic rubidium salts.[58] From these data it is not possible to determine whether the shifts in the resonances are related to 1D structural changes, or changes in paramagnetism arising from varying amounts of electrons in the conduction band of a metallic phase, as may be expected given the dramatic differences in conductivity between the $n = 3.0$ and $n = 4.0$ materials.

Discussion

Solid-state ^{87}Rb NMR spectra indicate that two major Rb environments exist within these materials: (i) Rb ions in the channels and (ii) Rb ions confined within the wall of the mesostructure. In addition, there are other resonances corresponding to Rb ions strongly associated with the various fulleride species, Rb ions in unique coordination environments in the tantalum oxide framework and channels, as well as the possibility of Rb ions associated with a rubidium tantalate phase at higher levels of reduction. These results are distinct from those of the previous ^{23}Na NMR investigation of analogous Na_3C_{60}/mesoporous tantalum oxide materials, in which channel and framework ions were observed in the ^{23}Na NMR spectra of all samples, and Na ions associated with fulleride species were only clearly resolved for the parent composite. However, in both the Na and Rb systems, there is a notable increase in alkali-metal cations associated with the mesostructure as the degree of reduction is increased. This trend could also be verified by XPS, where increased occupation of the sites associated with the walls of the mesostructure was associated with a decrease in binding energy of the Ta 4f 7/2 and 5/2 emissions. Because of the high degree of nonstoichiometry in these composite materials, as evidenced by solid-state ^{13}C NMR, a direct comparison of the composites with bulk fulleride materials is not possible. Apparently the absolute carbon loading level does not strongly contribute to the conductivity of our composites because the $n = 4.0$ material is more highly conductive than its $n = 1.0$ congener, despite having almost 50% less carbon in the pores. This suggests that the conductivity in these composites is due to the presence of certain fulleride species at certain oxidation states or a mixture of oxidation states as is evidenced from solid-state ^{13}C NMR.

The insulating behavior of the mixed oxidation state $n = 3.0$ composite is surprising, since this composite is only nominally an $n = 3.0$ material and contains only trace amounts of C_{60}^{3-}, always linked with insulating behavior in these materials.[16,17] The presence of several fulleride species and a high enough loading level of carbon to ensure the possibility of conductivity always leads to conducting behavior in the Na/Ta system, presumably through a polaron mechanism. The insulating behavior of this $n = 3.0$ composite may still be related to the presence of small insulating pockets of C_{60}^{3-} which act as bottlenecks to electron flow through the pore system; however, the $n = 4.0$ sample is a semiconductor and contains a significant amount of this species as well, making this explanation unlikely. The fact that this composite had a Raman signature consistent with $n = 3.0$, yet contained a variety of fulleride species, very little of which was C_{60}^{3-}, also calls into question the use of this technique alone to adequately characterize fulleride species in the pores, and possibly even in bulk materials. This also may shed light on many controversies in bulk fullerides, normally characterized by XRD and Raman, since Raman cannot assign an exact oxidation state, and XRD is unable to locate local islands of nonstoichiometry which may exist. In addition, the rate at which the vibrational frequency of fulleride softens depends on the class of fulleride materials and likely differs between bulk alkali-metal fullerides and our composite materials.

The most meaningful comparison in all of our work on mesoporous transition-metal oxide one-dimensional fulleride composites is between the $n = 3.0$ composite in the Na/Ta system and the bulk $n = 3.0$ fullerides, since this composite material showed an exclusive presence of C_{60}^{3-} with no other fulleride species and possessed a carbon loading level high enough to preclude insulating behavior due to a low concentration of charge carriers in the pores. At room temperature where low-dimensional lattice distortions are usually suppressed due to a high degree of molecular vibrations (except cases with a high degree of structural constraints, such as VO_2), this material is highly insulating. This suggests that the $n = 3.0$ phase is indeed a Mott−Hubbard insulator and one-dimensional confinement is not responsible for the low conductivity. This picture is in accord with theories that K_3C_{60} is a hole-doped Mott−Hubbard insulator analogous to the copper oxide superconductors. One caveat is that charge density waves form particularly easily in systems with half-filled bands (e.g., polyacetylene), and thus low-dimensional lattice distortions should be more favorable for the $n = 3.0$ Na−Ta sample. Since these materials are largely amorphous, unequivocally assigning $C_{60}-C_{60}$ distances to determine the presence of charge density waves may not be possible. The ^{13}C NMR of this material has sharp resonances consistent with fast motion, further favoring a picture where charge density waves are not formed at room temperature.

Conclusion

We have synthesized a new series of mesoporous tantalum oxide rubidium fulleride intercalates and studied their electronic properties as a function of rubidium loading level. Solid-state ^{87}Rb studies revealed two distinct Rb sites in all composites with progressive accumulation of the framework Rb ions at higher Rb loading levels, as well as unique Rb sites associated with a variety of fulleride species. ^{13}C NMR indicated the presence of numerous C_{60} species, underscoring the complexity of this system and the necessity of applying solid-state NMR conjointly with Raman spectroscopy. Quantitative comparison of fulleride oxidation states in the pure fullerides and fullerides in the composite materials is very

(58) Skibsted, J.; Jakobsen, H. J. *J. Phys. Chem.* **1999**, *103*, 7958.

challenging, since multiple oxidation states exist in the latter, and the two classes of materials are distinct in terms of their dimensionality. The comprehensive characterization presented herein and other related studies have certainly cast light onto further unusual structural and electronic properties of alkali-metal fullerides.

Acknowledgment. The donors of the Petroleum Research Fund, administered by the American Chemical Society, are thanked for funding. NSERC and the Ontario Premiere Research Excellence Program are also thanked for financial support. Lowell Wenger from Wayne State Michigan University is thanked for his help with XPS and variable-temperature measurements. R.W.S. thanks the Canadian Foundation for Innovation (CFI), the Ontario Innovation Trust (OIT), and the University of Windsor for funding the solid-state NMR laboratory. The Centre for Catalysis and Materials Research (CCMR) at the University of Windsor is also acknowledged for student support.

Supporting Information Available: ^{87}Rb MAS and static NMR spectra of mesoporous tantalum oxide reduced with 0.5 equiv of rubidium naphthalene in the absence of C_{60} (PDF). This material is available free of charge via the Internet at http://pubs.acs.org.

CM048174T